An advanced complementary scheme of floating photovoltaic and hydropower generation flourishing water-food-energy nexus synergies

Yanlai Zhou[a, c], Fi-John Chang[a,]*, Li-Chiu Chang[b], Wei-De Lee[a], Angela Huang[a], Chong-Yu Xu[c], Shenglian Guo[d]

[a.] Department of Bioenvironmental Systems Engineering, National Taiwan University, Taipei, 10617, Taiwan.
[b.] Department of Water Resources and Environmental Engineering, Tamkang University, New Taipei City, 25137, Taiwan.
[c.] Department of Geosciences, University of Oslo, P.O. Box 1047 Blindern, N-0316 Oslo, Norway.
[d] State Key Laboratory of Water Resources and Hydropower Engineering Science, Wuhan University, Wuhan 430072, China.

Correspondence to: Fi-John Chang (changfj@ntu.edu.tw).

Abstract

Hybrid hydropower and floating photovoltaic power generation has far-reaching effects on the intertwined water, food and energy (WFE) nexus, but the complementary operation is fundamentally challenging especially under high uncertainties of hydro-meteorological conditions. This study proposed an artificial intelligence-based WFE system-overarching solution driven by hybrid hydro-floating photovoltaic power generation for promoting nexus synergies. A multi-objective optimization model grounded upon the Grasshopper Optimization Algorithm was developed to simultaneously maximize hydro-floating photovoltaic power output, the ratio of water storage to reservoir capacity, and the ratio of water supply to water demand. The Shihmen Reservoir watershed and its WFE system in northern Taiwan constituted the case study. The results demonstrated that the proposed optimization model could significantly improve synergistic benefits of the WFE nexus by reaching 13%, 13.3% and 15.1% in water storage, food production and hydro-floating photovoltaic power output, respectively. The optimal tilt angles of floating photovoltaic installation would vary between -11.9° (Summer) and 44.3° (Winter). This study opens up new perspectives on green energy production expansion while stimulating WFE nexus synergies in support of policy-makers with feasible schemes on floating photovoltaic deployment in the interest of social sustainability. In consequence, new niches are exploited for floating photovoltaic deployment and give rise to impact mitigation concerning hydro-meteorological uncertainties on WFE nexus management.

Keywords: Floating photovoltaic; Hydropower generation; Water allocation; Multi-Objective Grasshopper Optimization Algorithm; Taiwan

Nomenclature

Abbreviations

AFP	annual food production
APB	annual power benefits
GW	gigawatts
WFE	water-food-energy
MJ	megajoule
MOGOA	multi-objective grasshopper optimization algorithm
MW	megawatts
MWh	megawatts-hour
PHO	floating PV and hydropower output
PV	photovoltaic
RSD	ratio of water supply to water demand
RWS	ratio of water storage to reservoir capacity
SOP	standard operation policy
USD	United States dollars

Indices

t	index of time, from 1 to n
a	index of crops, from 1 to m
i	index of solution in grasshopper population ($i \neq j$), from 1 to N_{pop}
j	index of solution in grasshopper population, from 1 to N_{pop}
k	index of iterations, from 1 to I_{max}
d	index of decision variables, from 1 to D

Parameters

c_{max}	maximal value of the decreasing coefficient
c_{min}	minimal value of the decreasing coefficient
C_T	transformation coefficient from temperature to power for modules of solar cell
D	number of decision variables
f	attraction intensity
g	gravity acceleration
I_{max}	maximal number of iterations
l	attractive length scale
LB_d	lower bound of decision variables in the d-th dimension
m	number of crops
M	number of year
n	number of time step
N_{pop}	size of population
N_{min}^h	minimum hydropower output
N_{max}^h	maximum hydropower output
N_{max}^p	maximum power output of floating PV
N_{min}^{ph}	minimum value of the total power output of floating PV and hydropower
N_{max}^{ph}	maximum value of the total power output of floating PV and hydropower
R_{min}	minimum water release
R_{max}	maximum water release
S_{min}	minimum reservoir storage
S_{max}	maximum reservoir storage
SR_{stc}	solar radiation intensity under standard test conditions
T_{stc}	air temperature of the standard test conditions (25 ℃)
UB_d	upper bound of decision variables in the d-th dimension
λ_{IR}	ratio of water supply to water demand of irrigation sector

λ_{PUB}		ratio of water supply to water demand of public sector
θ_0		specific solar incidence angle under the conditions ($\alpha_t = 0$ and $\gamma = 0$)
ϕ		latitude of floating PV deployment
γ		azimuth angle of floating PV deployment
δ		sun declination angle of floating PV deployment
ω		solar hour angle of floating PV deployment
η		efficiency coefficient of hydropower plant
ρ		density of water
Δt		time-step, at a scale of ten days
Δt_p		time-step in floating PV power generation (= average sunshine hours in a ten-day period)
Δt_h		time-step in hydropower generation at a scale of ten days

Variables

A_a		annual irrigation area of the a-th crop
$\hat{\mathbf{B}}_d$		vector of the best solution in the d-th dimension
c_k		decreasing coefficient at the k-th iteration
H_t		hydraulic head of hydro-turbine in the t-th time
I_t		reservoir inflow in the t-th time
N_t^h		power output of the hydropower in the t-th time
N_t^p		power output of the floating PV in the t-th time
N_t^{ph}		total output of the floating PV and hydropower in the t-th time
PU_a		annual food yield per unit of area (e.g. hectare) of the a-th crop
R_t^{ECO}		water release from the reservoir to satisfying river basic eco-flow in the t-th time
R_t^{IR}		water release from the reservoir to irrigation sector in the t-th time
$R_{t,a}^{IR}$		water release from the reservoir to the a-th crop in the t-th time
R_t^{PUB}		water release from the reservoir to public sector in the t-th time
R_t^{SP}		water release through reservoir spillway in the t-th time
R_t^{TOTAL}		total water release in the t-th time
RT_t		hydro-turbine inflow of hydro-turbine in the t-th time
S_t		reservoir storage in the t-th time
SR_t^{θ}		effective solar radiation intensity of the floating PV in the t-th time
SR_t		observed solar radiation intensity in the t-th time
T_t		air temperature of cell module in the t-th time
$WD_{t,a}^{IR}$		water demand of the a-th crop in the t-th time
WD_t^{IR}		water demand of irrigation sector in the t-th time
WD_t^{PUB}		water demand of public sector in the t-th time
x_i		current vectors of the i-th grasshopper ($i \neq j$)
x_j		current vectors of the j-th grasshopper
x_i^d		current vectors of the i-th grasshopper in the d-th dimension
x_j^d		current vectors of the j-th grasshopper in the d-th dimension
$\mathbf{X}_i^d$		next position vector of the i-th grasshopper in the d-th dimension
θ_t		solar incidence angle in the t-th time
α_t		tilt angle of floating PV deployment in the t-th time

4

1. Introduction

Global population growth, booming economy and urbanization leads to a rapid increase in demands for water, food and energy. The growing demands and interdependences among these precious resources produce stress hotspots in many societies and countries. Water-Food-Energy (WFE) nexus research seeks to explore and minimize tradeoffs among various dimensions of resources consumed by societies. WFE nexus management therefore plays an important role in sustainable development in the context of resource efficiency promotion and environmental threat mitigation. WFE nexus management nowadays attains an unprecedented height and tends to make tradeoffs among demands, purposes, benefits, human beings and environmental sustainability [1,2]. Technological solutions from water-, food-, and energy-driven perspectives [3,4] as well as the mixtures of the three perspectives [5] are being given full play to the reduction of greenhouse gas emission and the improvement of the mutual benefits of WFE sectors. Growths in WFE demands and greenhouse gas emissions compel global energy production to move toward a cleaner path. The collaborative operation among renewable energies (e.g. hydropower, solar power, and wind power) is currently being explored throughout the world to fulfill future targets of green economy [6,7] and sustainable development [8]. Due to meteorological uncertainties, larger output fluctuations appear in solar and wind power generation than in hydropower generation. In this background, owing to the superior regulation ability and flexibility of hydropower operation [9,10], the complementary operation between hydropower and solar power generation is regarded as one of the most promising solutions to increasing energy efficiency [11,12]. Furthermore, floating photovoltaics (PV) deployed on water directly is a rapidly developing emerging technology [13,14] and would be a plausible solution

5

instead of ground-mounted PV due to limited ground space and roof space [15,16].

Traditional ground-mounted PV installation and emerging water-based PV installation are two basic types of PV deployment technologies [17]. In comparison with ground-based PV deployment, water-based PV deployment can be additionally beneficial, such as reducing solar power production costs, increasing the efficiency in temperature regulation of PV modules, lowering water surface evaporation and algae growth, and potentially improving land conservation [18]. Competitive land uses and recognizable synergistic benefits in close relation to water-based floating PV deployment are contributing to facilitating this new niche application and development [19]. Heretofore, man-made water bodies, for instance, wastewater treatment, tailing, retention, and agricultural irrigation ponds and reservoirs, have become predominant sites of floating PV installation [20,21]. In 2007, the first floating PV system designed by the Japan National Institute of Advanced Industrial Science and Technology was installed in Japan while the first commercial floating PV system designed by the US Thompson Technology Industries was installed at the Far Niente Winery in California [18]. In 2018, the World Bank reported that the global floating PV potential was estimated up to 400 GW (gigawatts) with an installed capacity of approximately 300 MW (megawatts) to date [22]. According to the statistics of global top 100 floating PV projects [23], the total installed capacity reaches as much as 242.89 MW, where 98% is contributed by Japan (54%), China (32%), South Korea (8%) and the United Kingdom (4%) (Fig. 1(a)). The top 4 floating PV providers are Ciel & Terre (1st), Reservoir Solar Company (2nd), Takiron Engineering (3rd), and Sumitomo Mitsui Construction (4th) accordingly (Fig. 1(b)).
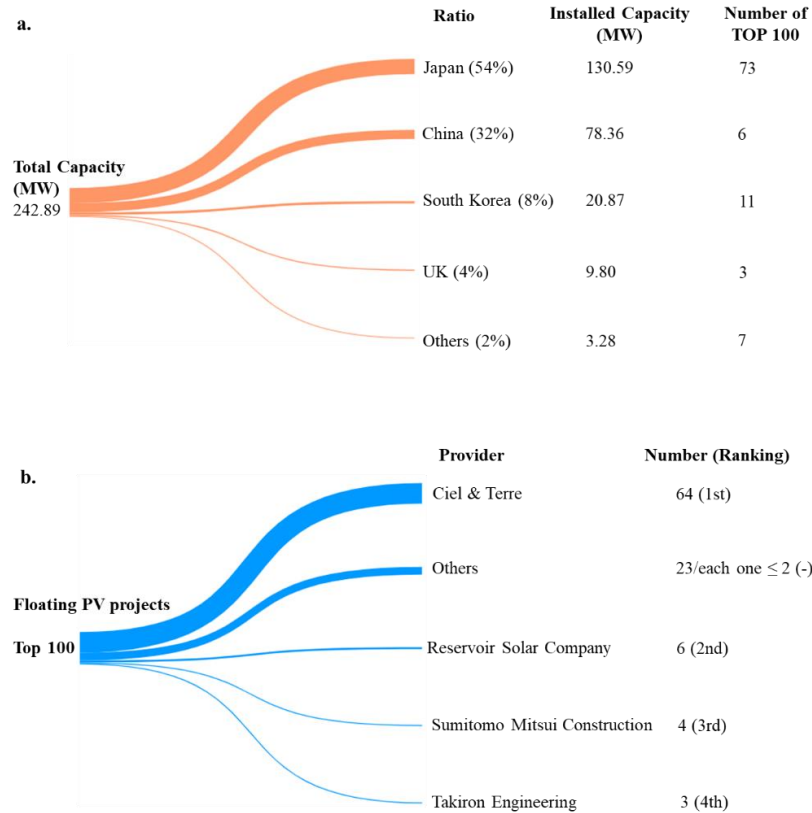
Fig. 1. Statistics of global top 100 floating PV projects. a. profile of installed capacity. b. ranking of floating PV providers. Data extracted from the Global Top 100 Floating Solar Projects [23].

Additionally, the largest (located at Huainan City in China) and the smallest (located at Aisai City in Japan) providers have an installed capacity of 40 MW and 460 kW, respectively. Despite that more and more countries like Japan and China are pursuing the scheme of deploying PV on man-made water bodies [18,23], current water-mounted floating PV projects have installed capacities smaller than ground-mounted ones while floating PV power generation has higher output uncertainty than hydropower generation. Therefore, it is interesting and meaningful to integrate regulatable hydropower generation with non-regulatable PV power generation to pursue their mutual benefits for maintaining stable power supply.

The collaborative operation between hydropower and PV (ground- or water-mounted) power generation would produce far-reaching influences on WFE nexus management, but such complementary implementation is fundamentally challenging because of hydrological and meteorological uncertainties and PV power's randomness, intermittency and fluctuation [24,25]. Researches with regard to collaborative operation between hydropower and PV power generation paid attention mainly to three aspects: optimization of power output of hydropower plants [26] and ground-based PV installation (not water-mounted PV) [27,28], impact assessment of floating PV deployment at reservoirs on hydropower operational flexibility [29] and water quality [30,31], and incorporation of hydropower [32,33] and/or PV power generation [34] into hybrid energy systems [35,36] or WFE nexus management [37,38]. For instance, Zhang et al. constructed an optimization model for chasing the complementary operation between hydropower and ground-mounted PV in response to different characteristics of energy demands and reservoir operation [24]. Ming et al. combined simulation and optimization approaches to adjust hydropower operation rule curves by considering the inputs of photovoltaic power production [25]. Haas et al. assessed the impacts of floating PV deployment on reservoir water quality, algal blooms, and hydropower output with respect to various water and power price conditions [29]. Stiubiener et al. proposed a hydropower-floating PV simulation model to improve the flexibility of hydropower operation [30]. Château et al. developed a system dynamic simulation model for evaluating the potential of floating PV installation over fish ponds through searching the optimal percentage of water surface covered by solar panels [31]. Yang et al. formulated a dynamic programming model to ameliorate the complementary operation between hydropower and ground-mounted PV [32]. Wang et al. configured a

8

two-objective optimization model to reduce the fluctuations of ground-mounted wind and solar power outputs through hydropower operation [33]. Uen et al. constructed a reservoir optimization model to raise the synergies of the WFE nexus by the collaboration between short-term hydropower operation and long-term water supply from irrigation ponds [37]. Zhou et al. proposed a bi-objective optimization model to improve WFE nexus management through optimizing multi-sectoral water allocation and small-hydropower deployment [38].

Research gaps among the aforementioned aspects were summarized. From the standpoint of water-mounted PV application, previous researches mainly concentrated either on ecological assessment using simulation techniques or on the optimal design of solar panels whereas few involved the optimization of hydropower and floating PV power outputs. From the standpoint of WFE nexus optimization (i.e. tri-objective optimization), previous researches focused either on bi-objective optimization techniques or on decomposition optimization techniques whereas few directly involved tri-objective optimization techniques. In other words, bi-objective and/or decomposition optimization techniques commonly decomposed a tri-objective optimization problem into several sub-optimization problems (i.e. a single-objective sub-problem and a bi-objective sub-problem, or three single-objective sub-problems), yet they would not solve the tri-objective optimization problem directly.

The novelty of this study relies upon the optimization of both floating PV deployment on irrigation ponds and existing hydropower operation using an innovative artificial intelligence technique, meanwhile, its application for the first time to spur on the synergies of the WFE nexus. Main contributions could be attributed to three aspects. First, the

9

mathematical model for tri-objective optimization was configured to simultaneously maximize hydropower and floating PV power outputs, the ratio of water storage to reservoir capacity, and the ratio of water supply to water demand. Second, the optimal hydropower generation, floating PV deployment, and multi-sectoral water allocation under various hydrological and meteorological conditions were obtained by adopting a nature-inspired optimization algorithm. Third, WFE synergies relating to the optimal solutions were acquired from the optimal hydropower operation in connection to the optimal floating PV deployment under three representative scenarios constituted by various hydrological and meteorological conditions. The theoretical framework proposed in this study not only creates new niches on green energy production and promotes WFE nexus synergies but also supports policy-making with feasible schemes on floating photovoltaic deployment in the interest of social sustainability. The Shihmen Reservoir and its WFE system in northern Taiwan formed the case study.

2. Study area and materials

Fig. 2 illustrates the schematic diagram of the water supply system (including irrigation ponds), agricultural irrigation areas and energy generation facilities located in the Shihmen Reservoir watershed. The Shihmen Reservoir situated in northern Taiwan is the pivotal infrastructure serving multiple purposes for the Taipei and Taoyuan metropolitan areas as well as the Taoyuan and Shihmen irrigation areas. This reservoir embraces a watershed area of 763 km^2 and has an effective storage capacity of 203 million m^3. The maximum storage of the conservation pool (208 million m^3) corresponds to its normal water level (245 m) while the dead storage of the inactive pool (5 million m^3) corresponds to its dead

10

water level (195 m). This multi-purpose reservoir is operated to meet water demands of

public and irrigation sectors, produce hydroelectricity, and implement flood prevention

tasks, where each of the six floodgates and the two tunnel spillways holds its maximal

discharge capacity of 11400 m^3/s and 2400 m^3/s, respectively. Two hydropower units

installed in the Shihmen hydropower station of the reservoir have a total installed capacity

of 90 megawatts (= 2*45 MW), an annual power output of 230 million kWh, and the

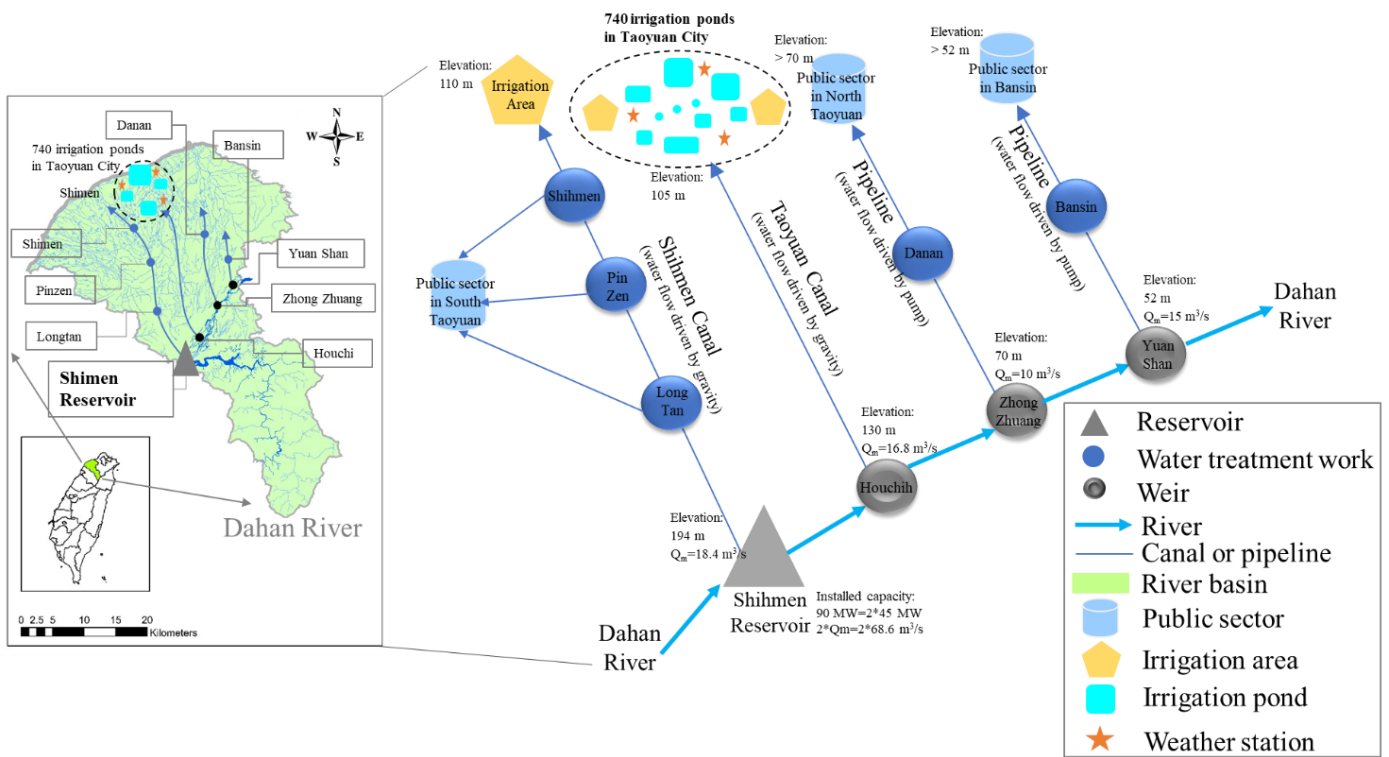maximal discharge of 137.2 m^3/s (= 2*68.6 m^3/s).

Fig. 2. Schematic diagram of the water supply system (including irrigation ponds), agricultural irrigation areas, and energy generation facilities located in the Shihmen Reservoir watershed, where floating PV devices would be deployed over 740 irrigation ponds in Taoyuan City. Q_m is the maximum discharge.

The Shihmen watershed contains the Dahan River basin and tributary basins, where

the Taoyuan and Shihmen irrigation areas occupy 270 km^2 and 121 km^2, respectively. The

mean annual precipitation of this watershed is close to 2500 mm, and seasonality of typhoon-induced floods spans from July to September basically. The routine operation of the Shihmen Reservoir is managed to supply water to various demanding sectors. Water released from the reservoir travels through the watershed via the Shihmen hydropower station, the Houchih Weir, and weirs located in the Dahan River whilst water also discharges from the reservoir into the Shihmen Canal to meet the water demands of public and irrigation sectors in South Taoyuan (Fig. 2). The remaining water would be released from spillway gates to the Houchih Weir as soon as possible when the water demands of public and irrigation sectors in the study area excluding South Taoyuan surpass the maximal discharge capacity (137.2 m^3/s) of the two hydropower plants.

Standard Operation Policy (SOP)

The authority of the Shihmen Reservoir will perform M-5 rule curves [37] if water conflicts occur between public and irrigation sectors. The SOP is introduced briefly, shown below.
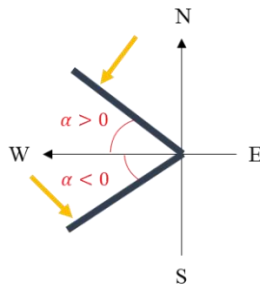
(a) The water supply system would completely meet water demands when the storage capacity of the Shihmen Reservoir is higher than the lower limit curve. Accordingly, the ratio (λ_{IR}) of water supply to irrigation water demands is equal to 1 meanwhile it is the same for the public sectors (λ_{PUB}=1).

(b) The values of λ_{PUB} and λ_{IR} are equal to 0.9 and 0.75, respectively, when the storage capacity of the Shihmen Reservoir situates between the critical lower limit curve and the lower limit curve.

(c) The values of λ_{PUB} and λ_{IR} are equal to 0.8 and 0.5, respectively, when the storage capacity of the Shihmen Reservoir falls below the critical lower limit curve.
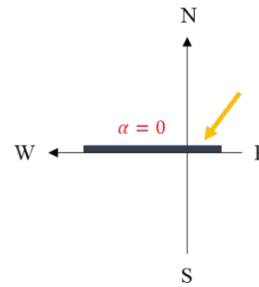
Floating PV deployment

A great deal of (740) irrigation ponds (volume of each pond $\geq$ 20 m (length)*5 m (width)*1 m (depth)) distributed across Taoyuan City possess an approximate cumulative capacity of 62 million m^3 and a total area of 12 km^2 (Fig. 2), and they would be regarded as the water bodies suitable for floating PV deployment (Fig. 3). The annual sunshine duration in Taoyuan City varies between 1400 and 2200 hours. In this study, the deployment of floating PV systems did not consider the impacts of PV types and their combinations on power output while the percentage of water surface of a pond covered with the floating PV system was set as 40% (i.e. installed area-to-pond area ratio) according to our previous study and the official announcement regarding the maximal pond area allowing PV deployment in Taiwan [31]. A floating solar system with Hydrelio polyethylene designed by Ciel & Terre (https://www.ciel-et-terre.net/) is considered for floating PV installation over these 740 ponds in this study. The Neo Solar power (DP310B4A) solar panel installed in this floating PV system (Fig. 3(a)) embraces an installed capacity of 310 W/unit, a size of 1.5 m^2/unit (= 1.5 m (length)* 1 m (width)), a tilt angle (α) relative to the horizontal, and a cost of 80 USD/unit (https://www.ciel-et-terre.net/). Consequently, in the case of an installed area-to-pond area ratio of 40%, a total installed capacity of 992 MW (= 12 (km^2)*40%/(1.5 m^2)*310 (W)) would be deployed over the 740 ponds (total area = 12 km^2) in Taoyuan City.

Fig. 3. Illustration of the floating PV system with an installed area-to-pond area ratio of 40% deployed over 740 irrigation ponds in Taoyuan City (α is the tilt angle of the floating PV deployment, relative to the horizontal). a. sketch map of floating PV deployment. b. Optimal tilt angle scheme with seasonal variation. c. traditional scheme of floating PV deployment under horizontal installation served as the benchmark.

In our previous study [31], both experimental comparison and mathematical simulation would lay a solid foundation for the high potential and practicality to deploy floating PV on ponds. Besides, based on the experimental data collected from ponds with (an installed area-to-pond area ratio of 40%) or without floating PV cover, the ecological impact assessment pointed out that the deployment of floating PV on ponds only has a

small negative impact on water quality by reason of a slight reduction in dissolved oxygen levels. The goal of floating PV deployment in this study was to search the optimal seasonal tilt angles to make a significant gain in solar radiation for maximizing solar panel efficiency (Fig. 3(b)). Additionally, the traditional scheme of floating PV deployment under horizontal installation (tilt angle = 0°) served as the benchmark (Fig. 3(c)). The purchase prices of hydropower and solar power in Taiwan in 2018 were 67 USD/MWh and 170 USD/MWh, respectively.

In this study, hydrological datasets were extracted from the Water Resources Agency in Taiwan (https://www.wra.gov.tw/, in Chinese), and meteorological datasets were extracted from the Central Weather Bureau in Taiwan (https://e-service.cwb.gov.tw/HistoryDataQuery/index.jsp, in Chinese). Hydrological datasets contained Shihmen Reservoir inflows of 15 hydrological years (July−the next June, 2004−2019) at a temporal scale of ten days (i.e. 36 ten-day periods*15 years) and the average water demands of two recent hydrological years (2017 and 2018) at a temporal scale of ten days (i.e. 36 ten-day period*1 year). Meteorological datasets consisted of average solar radiation intensity, average sunshine hours and average air temperature of three weather stations (Fig. 2), which were associated with 15 hydrological years (July−the next June, 2004−2019) at a temporal scale of ten days (i.e. 36 ten-day periods*15 years).

3. Methods

The kernel framework of WFE nexus management proposed in this study is presented in Fig. 4, involving two main parts. The multi-objective optimization model of the WFE
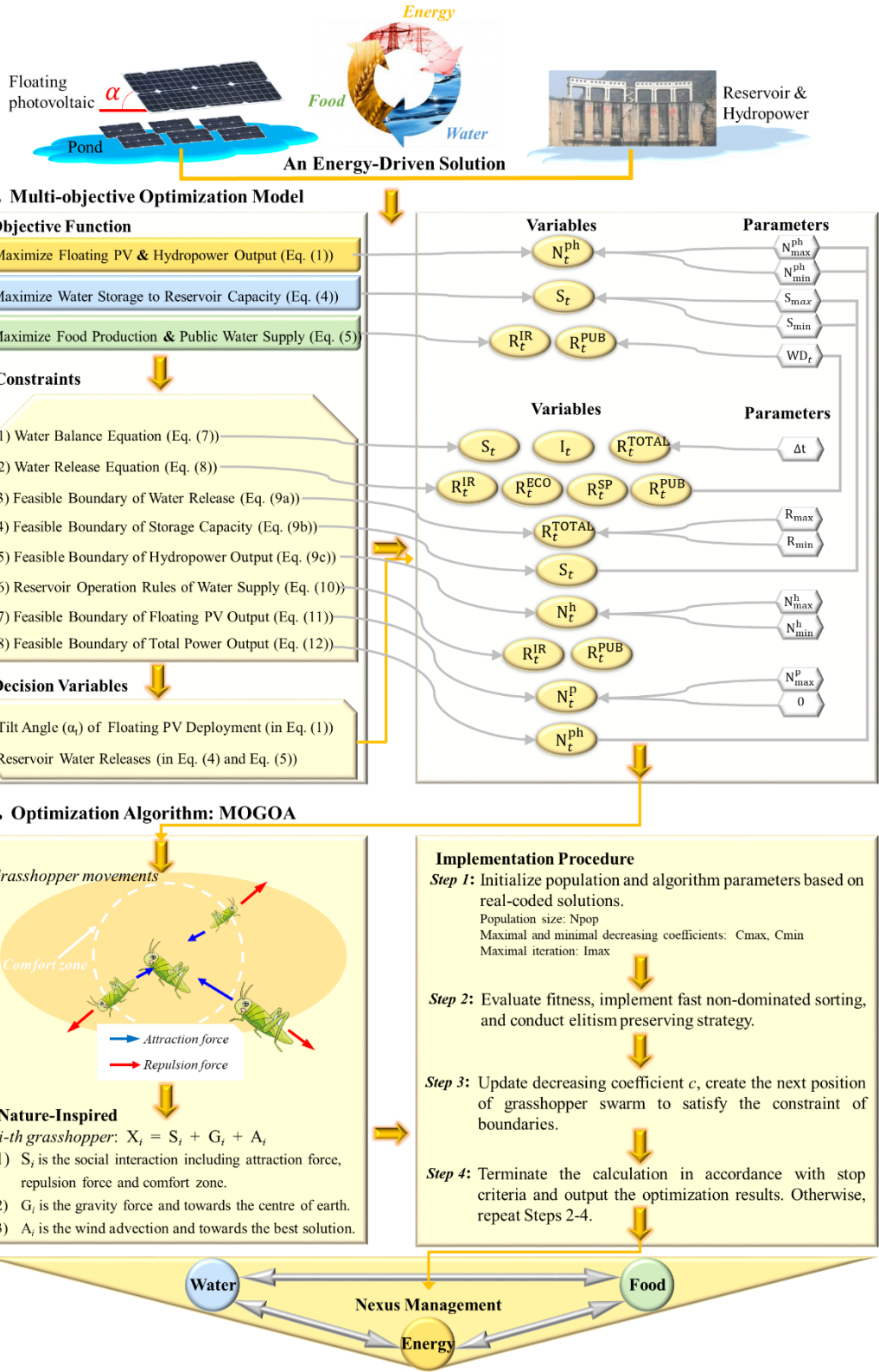
15

Fig. 4. Framework of Water, Food and Energy Nexus Management proposed in this study. a. Multi-objective optimization model. b. Multi-objective Grasshopper Optimization Algorithm (MOGOA).

nexus was configured at first by three objectives and relevant constraints so as to lift the floating PV and hydropower output, water supply reliability, and food production at the same time (Fig. 4(a)). Then the synergistic benefits of the WFE nexus were optimized using the Multi-objective Grasshopper Optimization Algorithm (MOGOA, Fig. 4(b)) driven by 15-year hydrological and meteorological circumstances at a ten-day scale. The methods adopted in this study are introduced briefly as follows.

3.1 Multi-objective optimization model of water-food-energy nexus

To tackle water-food-energy nexus challenges by increasing renewable power output meanwhile raising synergies between water and food sectors, this study proposes a multi-objective optimization model. The objective functions and variables of the mathematical model are summarized in Table 1. This model (Fig. 4(a)) is configured with Objective 1: maximization of average annual floating PV and hydropower output (PHO); Objective 2: maximization of average annual ratio of water storage to reservoir capacity (RWS); and Objective 3: maximization of average annual ratio of water supply to water demand of both public and irrigation sectors (RSD). The operation of hydropower plants should satisfy physical constraints, consisting of the reservoir water balance equation (Eq. (7)), the reservoir water release equation (Eq. (8)), the feasible boundaries of reservoir water release, reservoir storage capacity, and power output (Eqs. (9a), (9b) & (9c), respectively), as well as reservoir operation rules (Eqs. (10a) & (10b)), meanwhile, floating PV operation should obey the feasible boundaries of power output (Eq. (11)). Additionally, the plants of floating PV and hydropower should obey the feasible boundaries of power grid operation (Eq. (12)).

Table 1 summarization of variables and optimization objects of the multi-objective optimization model

17

Objective function		Item
Maximize PHO $= \frac{1}{M} \cdot \sum_{t=1}^{n} N_t^{ph} \cdot \Delta t = \frac{1}{M} \cdot (\sum_{t=1}^{n} N_t^p \cdot \Delta t_p + \sum_{t=1}^{n} N_t^h \cdot \Delta t_h)$ (1)		*Objective 1*: PHO
$N_t^p = N_{max}^p \cdot \left(\frac{SR_t^\theta}{SR_{stc}}\right) \cdot [1 + C_T \cdot (T_t - T_{stc})]$ (2a)		
$SR_t^\theta = SR_t \cdot \frac{\cos\theta_t}{\cos\theta_0}$ (2b)		
$\cos\theta_t = (\sin\phi \cdot \cos\alpha_t - \cos\phi \cdot \cos\gamma \cdot \sin\alpha_t) \cdot \sin\delta +$ $(\cos\phi \cdot \cos\alpha_t + \sin\phi \cdot \cos\gamma \cdot \sin\alpha_t) \cdot \cos\delta \cdot \cos\omega + \sin\gamma \cdot \cos\delta \cdot \sin\omega \cdot \sin\alpha_t$ (2c)		
$\cos\theta_0 = \sin\phi \cdot \sin\delta + \cos\phi \cdot \cos\delta \cdot \cos\omega$ (2d)		
$N_t^h = \eta \cdot \rho \cdot g \cdot RT_t \cdot H_t$ (3)		
Maximize RWS $= \frac{1}{M} \sum_{t=1}^{n} \left(\frac{S_t}{S_{max}}\right)$ (4)		*Objective 2*: RWS
Maximize RSD $= \frac{1}{M} \cdot \sum_{t=1}^{n} \left(\frac{R_t^{IR} + R_t^{PUB}}{WD_t^{IR} + WD_t^{PUB}}\right)$ (5)		*Objective 3*: RSD
AFP $= \frac{1}{M} \cdot \sum_{a=1}^{m} \left(\frac{\sum_{t=1}^{n} R_{t,a}^{IR}}{\sum_{t=1}^{n} WD_{t,a}^{IR}} \cdot PU_a \cdot A_a\right)$ (6a)		
$R_t^{IR} = \begin{cases} WD_t^{IR}, & if(R_t^{IR} > WD_t^{IR}) \\ R_t^{IR}, & else \end{cases}$ (6b)		
$\sum_{a=1}^{m} R_{t,a}^{IR} = R_t^{IR}, \qquad \sum_{a=1}^{m} WD_{t,a}^{IR} = WD_t^{IR}$ (6c)		
$R_t^{PUB} = \begin{cases} WD_t^{PUB}, & if(R_t^{PUB} > WD_t^{PUB}) \\ R_t^{PUB}, & else \end{cases}$ (6d)		

Constraints		Item
$S_{t+1} = S_t + (I_t - R_t^{TOTAL}) \cdot \Delta t$ (7)		Water balance equation
$R_t^{TOTAL} = R_t^{IR} + R_t^{PUB} + R_t^{ECO} + R_t^{SP}$ (8)		Water release equation
$R_{min} \leq R_t^{TOTAL} \leq R_{max}$ (9a)		Water release boundary
$S_{min} \leq S_t \leq S_{max}$ (9b)		Storage capacity boundary
$N_{min}^h \leq N_t^h \leq N_{max}^h$ (9c)		Power output boundary
$R_t^{PUB} = WD_t^{PUB} \cdot \lambda_{PUB}$ (10a)		Reservoir operation rules
$R_t^{IR} = WD_t^{IR} \cdot \lambda_{IR}$ (10b)		
$0 \leq N_t^p \leq N_{max}^p$ (11)		Floating PV boundary
$N_{min}^{ph} \leq N_t^{ph} \leq N_{max}^{ph}$ (12)		Power grid boundary

In objective 1:

N_t^p, N_t^h, and N_t^{ph} are the power output (megawatt, MW) of floating PV, the power output of the hydropower, and the total power output of floating PV and hydropower in the t-th time, respectively. n and M are the number of time steps and the number of years, respectively. Δt is the length of the time step (hours), and its value is set as ten-day ($\Delta t = \Delta t_h = 240$ hours) for hydropower generation while being set as average sunshine hours ($= \Delta t_p$) in a ten-day period for floating PV power generation. N_{max}^p is the maximum power output (MW) of floating PV. SR_t, SR_t^θ and SR_{stc} are the observed solar radiation intensity (MJ/m² (megajoule)) in the t-th time, the effective solar radiation intensity of floating PV with a solar incidence angle θ in the t-th time, and the solar radiation intensity under the standard test condition (i.e. temperature = 25 □), respectively. C_T is the transformation coefficient (/) from temperature to power for the modules of the solar cell. T_t and T_{stc} are the air temperature (□) of the cell module in the t-th time and the air temperature of the standard test condition (25 □), respectively. α_t is the tilt angle (°) of the floating PV deployment relative to the horizontal in the t-th time. ϕ, γ, δ, and ω are the latitude, the azimuth angle (°), the sun declination angle (°), and the solar hour angle (°) of floating PV, respectively, and they are constants for each pond. θ_t and θ_0 are the solar incidence angle (°) in the t-th time and the specific solar incidence angle (°) under the condition ($\alpha_t = 0$ and γ = 0), respectively. η, ρ, and g are the efficiency coefficient (/) of the hydropower plant, water density (kg/m³), and gravity acceleration (m/s²), respectively. RT_t and H_t are the hydro-turbine inflow (m³/s) and the hydraulic head (m) of the hydro-turbine in the t-th time, respectively. Eq. (2a) is modified according to the previous version developed by the U.S. National Renewable Energy Laboratory (NREL, https://www.nrel.gov/).

In objective 2:

S_t and S_{max} are the reservoir storage (m³) in the t-th time and the maximum reservoir capacity (m³), respectively. AFP and RSD are the annual food production (kg) and the ratio (/) of water supply to water demand in irrigation and public sectors, respectively.

In objective 3:

PU$_a$ and A$_a$ are the annual food yield (kg) of the a-th crop per unit area (hectare) and the annual irrigation area (hectare) of the a-th crop, respectively, and the crops involve rice, vegetables, and fruits in this study. m is the number of crops ($m = 4$, in this study). R$_{t,a}^{IR}$, R$_t^{IR}$, WD$_{t,a}^{IR}$, WD$_t^{IR}$, R$_t^{PUB}$, and WD$_t^{PUB}$ are the water release (m^3/s) from the reservoir to the a-th crop, the water release (m^3/s) from the reservoir to irrigation sectors, the water demand (m^3/s) of the a-th crop, the water demand (m^3/s) of irrigation sectors, the water release (m^3/s) from the reservoir to public sectors, and the water demand (m^3/s) of public sector in the t-th time, respectively. In this study, food production is considered as a mathematical function (Eq. (6a)) of food yield per unit area, irrigation area, and ratio of water supply to water demand variables, ignoring the impacts of sunlight and fertilization on food yield [39].

In constraints:

S$_t$ and I$_t$ are the reservoir storage (m^3) and reservoir inflow (m^3/s) in the t-th time, respectively. R$_t^{IR}$, R$_t^{PUB}$, R$_t^{ECO}$, R$_t^{SP}$, and R$_t^{TOTAL}$ are the water releases (m^3/s) from the reservoir to irrigation sectors, to public sectors, to satisfy ecological needs (river base flow), through reservoir spillways, and the total water release in the t-th time, respectively. R$_{min}$ and R$_{max}$ are the minimum and maximum water release (m^3/s), respectively. S$_{min}$ and S$_{max}$ are the minimum and maximum reservoir storage (m^3), respectively. N$_{min}^h$ and N$_{max}^h$ are the minimum and maximum hydropower output (MW), respectively. WD$_t^{PUB}$ and WD$_t^{IR}$ are the water demands (m^3/s) of public and irrigation sectors in the t-th time, respectively. N$_{max}^p$ is the maximum power output (MW) of the floating PV. N$_{min}^{ph}$ and N$_{max}^{ph}$ are the minimum and maximum total power outputs (MW) of floating PV and hydropower, respectively, while the latter relies on the maximal transmission capacity of the transmission line of the power grid.

According to the mathematical equations of this multi-objective optimization model, the first objective function (Eq. (1)) is closely linked with the decision variables of the tilt angle (α_t) of floating PV deployment and the reservoir water release through the hydro-turbine (RT$_t$), the second objective function (Eq. (4)) is closely associated with the decision variables of water release from reservoir to various water demanding sectors, and the third objective function (Eq. (5)) is closely related to the decision variable of water release from reservoir to irrigation and public sectors (R$_t^{IR}$ & R$_t^{PUB}$). That is to say, this model aims at searching for the optimal tilt angle (α_t) of the floating PV deployment and the optimal reservoir water releases to increase the synergistic benefits of the WFE nexus. The next section would introduce a multi-objective optimization algorithm to solve the proposed optimization model.

3.2 Multi-objective Grasshopper Optimization Algorithm (MOGOA)

The MOGOA firstly proposed by Mirjalili et al. [40] is an evolutionary algorithm derived

from the single-objective Grasshopper Optimization Algorithm [41]. The MOGOA models and mimics the interactive behavior of grasshopper swarm (Fig. 4(b)) characterizing attraction force, repulsion force, and comfort zone in nature for solving multi-objective optimization problems. The MOGOA has demonstrated its robustness and superiority in the optimization of multi-objective problems through testing various Pareto optimal fronts, including linear, nonlinear, convex, concave as well as separated ones [40], in comparison to well-recognized and popular multi-objective algorithms in the literature such as Non-dominated Sorting Genetic Algorithm-II [42], Multiple-objective Particle Swarm Optimization [43], Multi-objective Ant Colony Optimization [44], Multi-objective Differential Evolution [45], and Multi-objective Evolution Strategy [46].

This study would center on the exploration of the MOGOA for optimizing the WFE nexus, rather than on the comparison of various multi-objective optimization algorithms. That is to say, the MOGOA is implemented for the first time to provide energy-driven WFE nexus solutions through concurrently searching the optimal tilt angle (α_t) of floating PV deployment and the optimal reservoir operations needed to maximize the PHO (Eq. (1)), the RWS (Eq. (4)) and the RSD (Eq. (5)) during 2004 and 2019 (= 15 years). The implementation procedure of the MOGOA is illustrated in Fig. 4(b) and described as follows.

Step 1: Initialize a population of search agents (i.e. grasshopper swarm) possessing a size of N_{pop} randomly; and set the values of parameters of the maximal and minimal values of the decreasing coefficient and the maximal number of iterations. Real-coded solutions are used for the decision variables of the tilt angle (α_t) and reservoir water releases (R_t^{IR} & R_t^{PUB}).

Step 2: Evaluate the fitness values of grasshopper swarm; conduct the fast non-dominated

sorting for partitioning the grasshopper population into various ranks; compute the

crowding distance of the grasshopper population; implement the roulette wheel

operation to select the best solution possessing a higher value of fitness (i.e. the

elitism preserving strategy) for creating an offspring of the grasshopper population.

The size of the offspring population in every iteration should be N_{pop}.

Step 3: For the k-th iteration, update the value of the decreasing coefficient using Eq. (13);

map the distance between every two grasshoppers onto the interval of (0, 15] to

divide the space between grasshoppers into the attraction zone (0, 1], the comfort

zone (1, 4] and the repulsion zone (4, 15]; create the next positions of the

grasshopper swarm using Eq. (14); and bring back the current grasshopper swarm

if the swarm go outside the boundaries (e.g. (0, 15]).

$$c_k = c_{max} - k \cdot \frac{(c_{max} - c_{min})}{I_{max}} \tag{13}$$

$$\mathbf{X}_i^d = c_k \cdot \left(\sum_{\substack{j=1 \\ j \neq i}}^{N_{pop}} c_k \cdot \frac{(UB_d - LB_d)}{2} \cdot s\left(\left\| x_j^d - x_i^d \right\|\right) \cdot \frac{(x_j - x_i)}{\|x_j - x_i\|} \right) + \widehat{\mathbf{B}}_d \tag{14a}$$

$$s(x) = f \cdot e^{\frac{-x}{l}} - e^{-x} \tag{14b}$$

where c_k is the decreasing coefficient to minify the repulsion zone, comfort zone and

attraction zone at the k-th iteration. c_{max} and c_{min} are the maximal and minimal values of

c_k, respectively. $\mathbf{X}_i^d$ is the next position vector of the i-th grasshopper in the d-th dimension

($d = 1, 2, \dots, D$, and D is the number of decision variables) and is derived from its current

position, the position of the best solution, as well as the positions of all other grasshoppers.

UB_d and LB_d are the upper and lower bounds of decision variables in the d-th dimension,

respectively. x_i^d and x_j^d are the current vectors of the i-th grasshopper and the j-th

grasshopper in the d-th dimension, respectively. $\boldsymbol{x}_i$ and $\boldsymbol{x}_j$ are the current vectors of the i-th grasshopper and the j-th grasshopper, respectively. $\left\| x_j^d - x_i^d \right\|$ is the distance between the i-th grasshopper and the j-th grasshopper in the d-th dimension. $\frac{(x_j - x_i)}{\left\| x_j - x_i \right\|}$ is the unit vector from the i-th grasshopper to the j-th grasshopper. $\widehat{\mathbf{B}}_d$ is the vector of the best solution in the d-th dimension. $s(x)$ is defined as the function of social forces with variable x while the parameters of f and l are the attraction intensity and the attractive length scale, respectively.

Step 4: Terminate the calculation in accordance with stop criteria by assessing the solutions through Steps 2-4. If the iteration number is less than the maximum iteration (I_{max}), then perform Steps 2-4 repeatedly. Otherwise, stop iteration as well as output the optimization results.

The MOGOA model built for WFE nexus optimization is driven by a total of 1728 datasets (= 3 variables (reservoir inflow, solar radiation intensity and temperature)∗36 ten-day periods∗15 years + 3 water demands (public, irrigation and river basic eco-flow)∗36 ten-day periods), 1620 decision variables (= 3 variables∗36 ten-day periods∗15 years), and 4860 constraints (= 540∗7 (hydropower) + 540∗2 (floating PV)) (Fig. 4(b)). To obtain converged results, a trial-and-error procedure is carried out intensively to configure the parameters of the MOGOA. Therefore, the values of the population size (N_{pop}), the maximum iteration (I_{max}), the maximum and minimum decreasing coefficients (c_{max}, c_{min}), the attraction intensity (f), and the attractive length scale (l) are set as 1000, 500, 1, 0.0001, 0.5, 1.5 respectively, where each solution involves 1620 decision variables in this case.

4. Results and discussion

22

Fast development of urbanization and industrialization has triggered huge crises and challenges in the nexus management on water, food and energy demands. This study centered on probing into long term complementary operation between floating PV and hydropower to boost the synergistic benefits of the WFE Nexus with the use of artificial intelligence-based heuristic techniques. The details of results and key findings were presented and elaborated in three perspectives: optimization of water-food-energy nexus using MOGOA; synergy analysis of water-food-energy nexus; and summarization.

4.1 Optimization of water-food-energy nexus using MOGOA

The main objective of this study is to probe into the synergistic benefits of the WFE nexus motivated by floating PV and hydropower output optimization with the use of a novel nature-inspired algorithm (i.e. MOGOA) under a specified multiple-year (2004-2019) scenario at a temporal scale of ten days. Besides, a simulation-based approach (i.e. Eq. (2) with the tilt angle $\alpha_t=0°$, Fig. 3(c)) was adopted for calculating the floating PV power output while the Standard Operation Policy (SOP)-based approach (M-5 rule curves) was applied to estimating the outputs of water, food and hydropower, where the non-optimization technique (i.e. the combination of simulation-based and SOP) served as the benchmark for comparison purpose.

   Fig. 5(a) displayed 1000 non-dominated solutions concerning the multiple-year scenario, where solutions were distributed independently on the Pareto optimal front of three objectives (PHO, RWS and RSD) meanwhile converged at the 500th iteration. To better express the distribution pattern of Pareto optimal solutions, a surface interpolation was conducted over these discrete 1000 solutions (Fig. 5(a)). The resulting Pareto front surface displays a pretty smooth and upward convex shape, and the 1000 solutions well-fit

the interpolated surface. The results clearly pointed out the three objectives (PHO, RWS, and RSD) competed with each other. For instance, larger floating PV and hydropower outputs (PHO) would be accompanied in pace with smaller water storage volumes (RWS) and/or lower water supply reliability (RSD), and vice versa. That is to say, Solution A tended to be the circumstance completely dominated by PHO, Solution B was inclined to be the circumstance completely dominated by RWS, whereas Solution C seemed to be the circumstance completely dominated by RSD. The remaining solutions such as Solution D were marked as compromised solutions to facilitate tradeoffs among the three objectives.

The results demonstrated that the MOGOA could search and approximate to the best non-dominated solutions for the multi-objective optimization of the WFE nexus because of the solutions spreading with high coverage and superior diversity across three objectives (Fig. 5(a)) as well as the excellent convergence ability (Figs. 5(b)-(d)). The reasons for the MOGOA's good performance are summarized here. First, the high coverage is owing to the mechanism of target selection. Second, the superior diversity benefits from avoiding an overcrowded repository by discarding and replacing non-dominated solutions with new ones. Last but not the least, the excellent convergence ability is ascribed to the adaptive mechanism that stimulates the grasshoppers' behaviors in the direction of the Pareto optimal solutions.
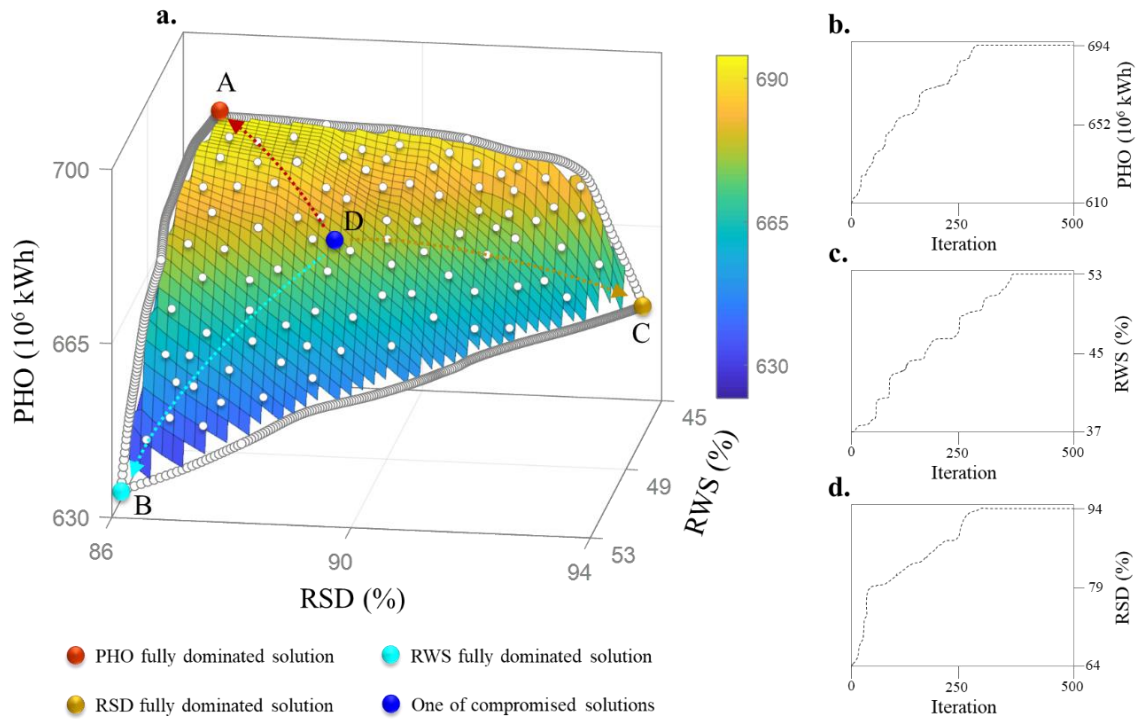
Fig. 5. Pareto front of the MOGOA (converged at the 500th iteration) concerning the floating PV and hydropower output (PHO), the ratio of water storage to reservoir capacity (RWS), and the ratio of water supply to water demand (RSD) under a multiple-year scenario (2004-2019). a. Optimal solutions to WFE nexus management, where the Pareto front surface interpolated was colored with gradient color. b-d. Iteration performance with respect to three objective functions.

Table 2 presented the optimal outputs of water, food and energy acquired from the MOGOA under the multiple-year scenario. It was easy to find that the MOGOA produced much better performances (larger RWS and RSD values, and higher average annual floating PV and hydropower output) than the non-optimization technique that combined simulation-based and SOP approaches. The results demonstrated that the optimal MOGOA solutions would substantially lift reservoir storage (RWS), significantly improve water supply reliability (RSD), and effectively increase floating PV and hydropower output (PHO) at the same time. The compromised solution (Solution D) could increase RWS, RSD and PHO by 6.5%, 8.4% and 12.4%, respectively. Additionally, the maximal improvement rates

25

in PHO (15.1%), RWS (13%), and RSD (13.3%) corresponded to the individual solutions under the circumstances completed dominated by PHO (Solution A), RWS (Solution B), and RSD (Solution C), respectively. In other words, the obtainments of the solutions completely dominated by PHO (Solution A), RWS (Solution B), and RSD (Solution C) were to implement the solution search in the directions towards maximizing PHO, RWS, and RSD, respectively. It was an interesting finding that the ranges of improvement rates in water (2.2%−13%), food (3.6%−13.3%) and energy (4.8%−15.1%) sectors were similar. This could be contributed by the synergistic optimization capability of the MOGOA, different from the optimization with just one objective or two objectives gaining top priority.

Table 2 Water, food, and energy outputs acquired from the MOGOA optimization (Fig. 5(a)) and the non-optimization technique under the multiple-year scenario.

Objective	Indicator	MOGOA[a] Pareto Optimal Solutions				Non-optimization[b] (benchmark)
		A	B	C	D	
Water	RWS[c]	48 (4.3[f])	52 (13.0)	47 (2.2)	49 (6.5)	46
Food	RSD[d]	87 (4.8)	86 (3.6)	94 (13.3)	90 (8.4)	83
Energy	PHO[e]	694 (15.1)	632 (4.8)	656 (8.8)	678 (12.4)	603

[a] Multi-objective Grasshopper Optimization Algorithm.

[b] A combination of simulation-based and Standard Operation Policy (SOP) approaches, where the simulation-based approach (i.e. Eq. (2) and the tilt angle α_t=0) was adopted for calculating the floating PV output while the SOP-based approach (M-5 rule curves) was applied to estimating the outputs of water, food and hydropower.

[c] Average annual ratio of water storage to reservoir capacity (%).

[d] Average annual ratio of water supply to water demand (%) ($\equiv$ annual food production).

[e] Average annual floating PV and hydropower output (10^6 kWh).

[f] Improvement rate (%), and the benchmark was the non-optimization technique.

Fig. 6 further illustrated the competition between objectives in pairs: (a) energy versus water; (b) energy versus food; and (c) water versus food. Point A represents the optimal solution merely maximizing the floating PV and hydropower output (Objective 1).

26

Point B represents the optimal solution exclusively deliberating water storage (Objective 2). Point C represents the optimal solution only considering water supply reliability (Objective 3). Point D represents a comprised solution. With the optimal solutions on hands, members of think tanks could effectively provide decision-makers with deliberate strategies to wisely manage the intensive conflicts among energy, food and water demanding sectors encountering various meteorological and hydrological conditions. For example, the optimal solutions close to Solution A were prone to maximizing the energy output (PHO), suggesting it would be adequate to implement floating PV deployment schemes and reservoir operation strategies corresponding to these optimal solutions in years with high solar radiation intensity and abundant precipitation, respectively. The optimal solutions close to Solution B was inclined to maximize the water storage (RWS), indicating it would be adequate to implement floating PV deployment schemes and reservoir operation strategies associated with these optimal solutions in years with low solar radiation intensity and less precipitation, respectively. The optimal solutions close to Solution C tended to maximize the water storage (RSD), recommending it would be adequate to implement floating PV deployment schemes and reservoir operation strategies related to these optimal solutions in years with low solar radiation intensity and abundant precipitation, respectively. Alternatively, the compromised solutions (Solution D in the blue dotted circle) tended to make tradeoffs between two objectives, implying it would be suitable to implement floating PV deployment schemes and reservoir operation strategies related to these optimal solutions in years with moderate solar radiation intensity and moderate precipitation, respectively.
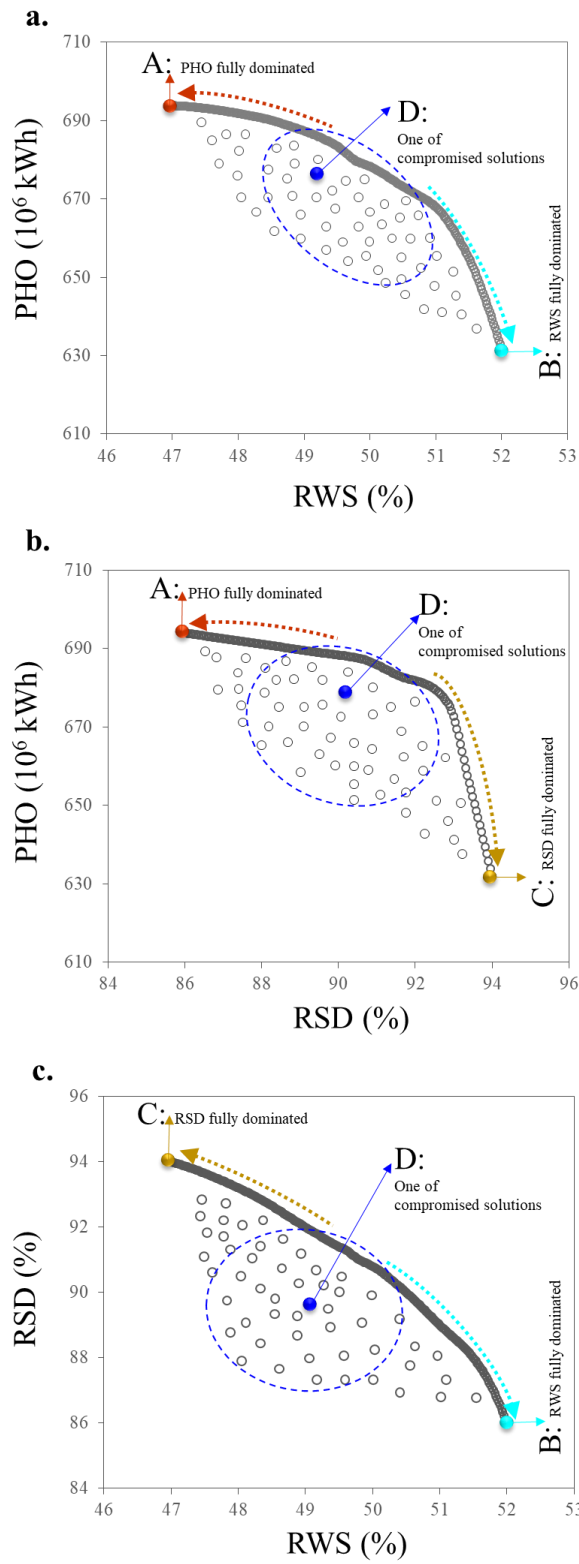
27

Fig. 6. Competition between objectives in pairs. a. Energy (PHO) versus Water (RWS), b. Energy (PHO) versus Food (RSD). c. Water (RWS) versus Food (RSD).

Table 3 presented the optimal results of floating PV and hydropower output acquired from the MOGOA in different seasons under the multiple-year scenario. As compared with the non-optimization technique, the MOGOA not only increased the hydropower output significantly but also raised the floating PV power output substantially. It was an interesting finding that floating PV schemes associated with the MOGOA made considerable improvements in seasonal power outputs, especially prominent in spring and summer. Hydropower generation strategies corresponding to the MOGOA also produced appreciable improvements in seasonal power outputs, especially noticeable in autumn and winter. Taking Solution A for example, the improvement rates of the floating PV power output not only reached 14.6% and 12.5% in autumn and winter accordingly but also achieved as high as 21.8% and 20.2% in spring and summer accordingly. The improvement rates of hydropower output attained 6.8% and 6.5% in spring and summer accordingly and reached as much as 16.7% and 10.3% in autumn and winter accordingly. There are two main reasons to achieve these outcomes. Despite that the floating PV is classified as non-regulatable energy, the optimal tilt angle (α_t) schemes could effectively develop the potential of solar power in four seasons and carve out a new niche for floating PV deployment to overcome meteorological uncertainty. Besides, the optimal water release strategies not only could prompt reservoir operation between flood season (summer) and non-flood season (winter) to be complementary but also could spur on the complementarity between hydropower and solar sources for reducing hydrological uncertainty. In addition, considering Taiwan's energy prices in 2018, the MOGOA solution greatly improved the average annual output of hydropower (10%) and floating PV (18.3%) as much as 91 million USD/yr.

29

Table 3 Floating PV deployment and hydropower output obtained from the MOGOA optimization (Fig. 5(a)) and the non-optimization technique (benchmark) in different seasons under the multiple-year scenario.

Power output[a] (10^6 kWh)	Period	MOGOA[b] Pareto Optimal Solutions				Non-optimization[c] (benchmark)
		A	B	C	D	
Floating PV	Spring	102 (20.2[d])	88 (4.8)	93 (10.7)	98 (16.7)	84
	Summer	173 (21.8)	152 (7.8)	161 (13.4)	168 (18.3)	142
	Autumn	97 (14.6)	88 (4.0)	91 (7.5)	95 (12.2)	85
	Winter	69 (12.5)	62 (1.0)	63 (2.7)	65 (6.0)	61
	Annual	440 (18.3)	390 (4.8)	408 (9.7)	426 (14.5)	372
Hydropower	Spring	47 (6.8)	45 (2.3)	46 (4.5)	47 (6.8)	44
	Summer	98 (6.5)	94 (2.2)	96 (4.3)	97 (5.4)	92
	Autumn	77 (16.7)	72 (9.1)	74 (12.1)	75 (13.6)	66
	Winter	32 (10.3)	31 (6.9)	32 (10.3)	33 (13.8)	29
	Annual	254 (10.0)	242 (4.8)	248 (7.4)	252 (9.1)	231

[a] Average seasonal power output of multiple years (2004-2019).

[b] Multi-objective Grasshopper Optimization Algorithm.

[c] A combination of simulation-based and Standard Operation Policy (SOP) approaches, where the simulation-based approach (i.e. Eq. (2) and the tilt angle $\alpha_t=0$) was adopted for calculating the floating PV output while the SOP-based approach (M-5 rule curves) was applied to estimating the outputs of water, food and hydropower.

[d] Improvement rate (%), and the benchmark was the non-optimization technique.

Though the computation time step in this study was set as a ten-day period, Fig. 7 only presented the monthly tilt angle (α_t) results (= the average tilt angle of three ten-day periods). The reason for setting the time interval of the dynamic control on tilt angle as monthly time step, rather than a season or ten-day, was owing to making the tradeoff between the improvement in photoelectric conversion efficiency and the reduction in operation cost of floating PV deployment. Fig. 7 revealed the optimal tilt angle (α_t) schemes of floating PV deployment in four seasons in Taoyuan City. It was easy to observe that the maximal positive tilt angle appeared in winter (January, 44.3°) whereas the maximal negative tilt angle occurred in summer (July, -11.9°). Tilt angles in spring
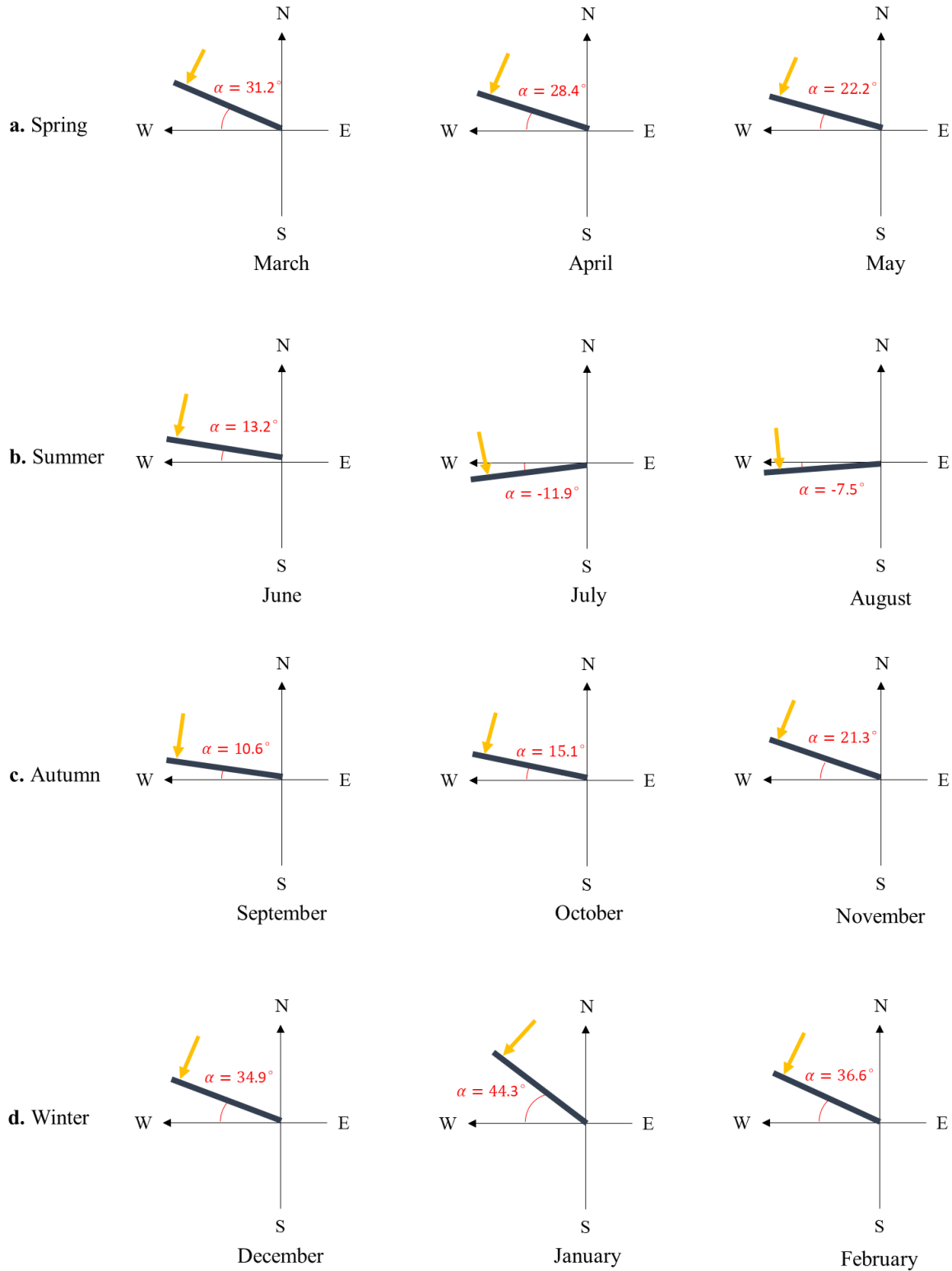
Fig. 7. Optimal tilt angle (α_t) schemes of floating PV deployment in four seasons in Taoyuan City. Yellow arrow denotes the vertical solar radiation for gaining the maximum solar radiation intensity. E: East. S: South. W: West. N: North.

and summer were positive and varied between 10.6° and 31.2°. Each optimal monthly tilt angle scheme aimed to maximize monthly photoelectric conversion efficiency through pursuing the maximal duration of vertical solar radiation (yellow arrow in Fig. 7) coupled with solar radiation intensity (i.e. different altitude angle, sun-earth distance and sunshine duration).

To mitigate the impacts of uncertainties concerning installation site and PV type on energy production cost in light of the Renewable Energy Statistics (2019) [22], production profits, installation cost and maintenance cost were taken into account for calculating the period of cost recovery in this study. The total installation cost of floating PV was considered to be funded by a 10-year loan with an annual interest rate of 5% by local banks. The annual maintenance cost was set as 3% of the initial cost of each floating PV panel [47]. Moreover, the installation cost also took the impacts of the panel slopes (=tilt angle) into account [19]. Based on production profits, installation cost and maintenance cost, the period of cost recovery would reach 8 years (10 years) subject to a minimum of 25-year (30-year) lifespan of floating PV. Under the optimal installed area-to-pond area ratio (40%) of floating PV deployment, a recommendation was made to install a total installed capacity of 992 MW (= 12 (km^2)*40%/(1.5 m^2)*310 (M)) sited in 740 ponds of Taoyuan City. Such floating PV deployment would need a total installed cost of USD 942.4 million (=992*950/1000 million USD) while bring an average annual floating PV benefit ranging between USD 66.3 million (= 390*1000 MWh*170 USD/MWh) in Solution B and USD 74.8 million (= 440*1000 MWh*170 USD/MWh) in Solution A (Table 2). For such cases in accordance with current renewable energy prices, the floating PV costs would be amortized over 8−10 years.

Despite the spatio-temporal heterogeneity of tilt angles, the reasons for this study to consider only temporal heterogeneity are two-fold: the spatial heterogeneity 【4313 MJ/m^2 (megajoule), 4396 MJ/m^2】 of average annual solar radiation intensity over 740 irrigation ponds (12 km^2 in area) is small; and the temporal heterogeneity 【661 MJ/m^2 (Winter), 1508 MJ/m^2 (Summer)】 of average seasonal solar radiation intensity in Taoyuan City is large.

4.2 Synergy analysis of water-food-energy nexus

Despite that there were 9 (=3∗3) scenarios in combinations of hydrological (Dry, Normal, and Wet years) and meteorological (High, Moderate, and Low solar radiation intensity) conditions, three scenarios were specified to assess the impacts of hydrological and meteorological uncertainties on synergetic benefits of the WFE nexus. S1 (Dry plus Low), S2 (Normal plus Moderate), and S3 (Wet plus High) represent poor, moderate, and good hydro-meteorological conditions, respectively.

Fig. 8 presented the synergetic benefits of the WFE nexus based upon the optimal MOGOA solutions under scenarios S1, S2, and S3, where the non-optimization technique (i.e. M-5 rule curves plus simulation-based) served as the benchmark. Though the MOGOA solutions could effectively raise the synergetic benefits of the WFE nexus in all the three scenarios, Solution A demonstrated to boost energy benefit greatly, Solution B demonstrated to increase water storage highly, and Solution C demonstrated to improve food production surpassingly. For instance, the cases upon Solutions (A, B, and C) under the Wet plus High scenario (S3: wet year and high solar radiation intensity; orange color in Fig. 8) would achieve the largest benefits: USD 93.9×10^6 for APB (energy sector), 55% for RWS (water sector), and 78×10^6 kg for AFP (food sector). In addition, Solution D was
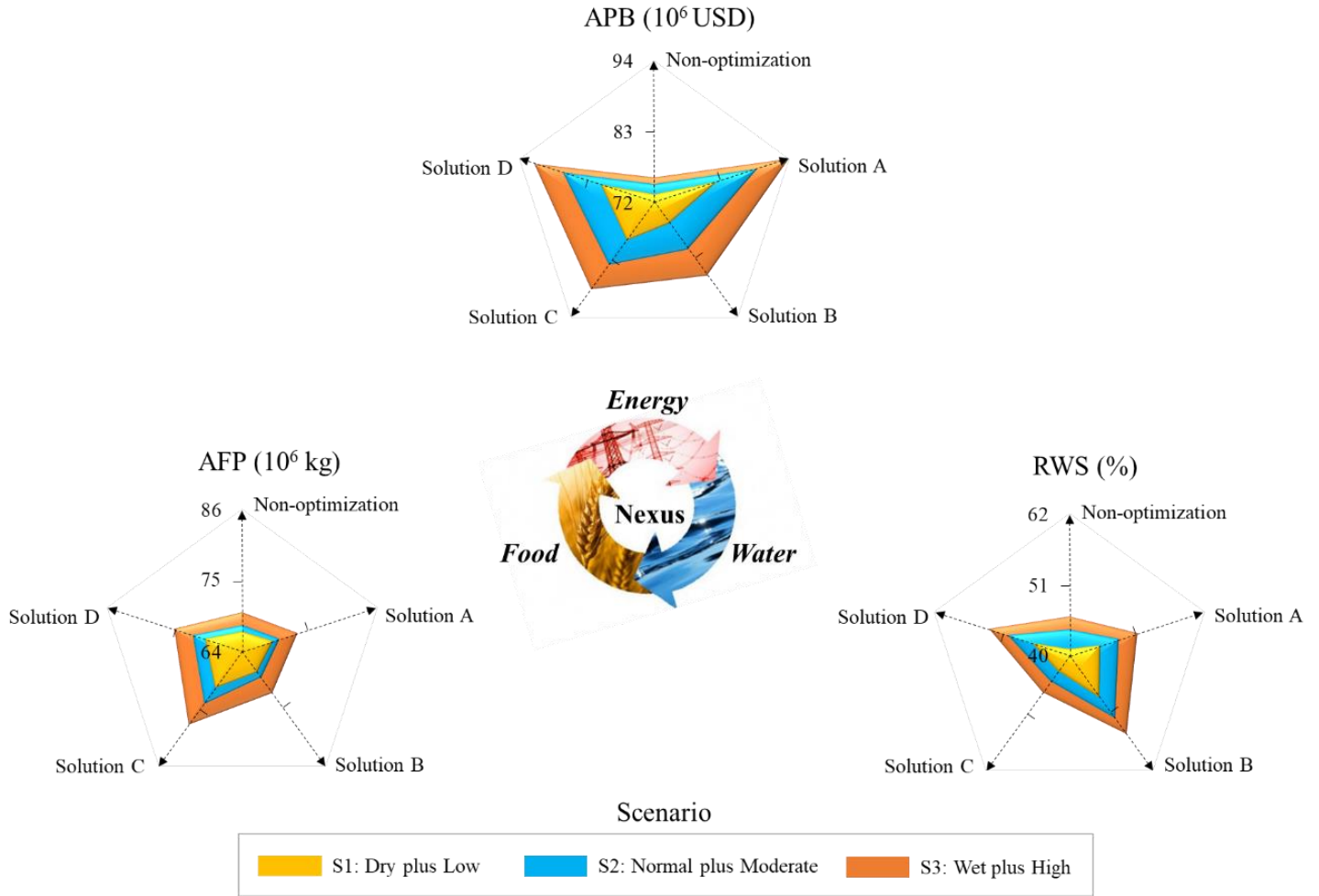
33

Fig. 8. Synergistic benefits of the WFE nexus based on the optimal MOGOA solutions (A, B, C, D) under three scenarios (S1, S2, S3). The non-optimization technique is the benchmark.

Scenario setting:

  S1_Dry (Low) year: occurrence frequency of a dry year (low solar radiation intensity) was 80% (80%) during 2004 and 2019.

  S2_Normal (Moderate) year: occurrence frequency a normal year (moderate solar radiation intensity) was 50% (50%) during 2004 and 2019.

  S3_Wet (High) year: occurrence frequency of a wet year (high solar radiation intensity) was 20% (20% during 2004 and 2019.

  Hydrological (meteorological) year: starting from July to the next June in the study area.

Indicators of benefits:

  APB (10^6 in USD): average annual power benefits of floating PV (in Taoyuan City) and hydropower (Shihmen Hydropower Station). Purchase prices of solar power and hydropower were 170 USD/MWh and 67 USD/MWh accordingly.

  RWS (%): average annual ratio of water storage to reservoir capacity in the Shihmen Reservoir.

  AFP (10^6 kg): average annual food production (including rice, vegetables, and fruits).

regarded as one of the compromised solutions and would hunt for the synergistic benefits of three sectors at the same time, rather than the benefit of one sector only. It was obvious that synergetic benefits were larger in the Wet plus High scenario (S3, orange color in Fig. 8) than in the Dry plus Low scenario (S1, yellow color in Fig. 8). It appeared that synergetic benefits in relation to the three scenarios were, as expected, ranked as: S3 (Wet plus High, orange) > S2 (Normal plus Moderate, blue) > S1 (Dry plus Low, yellow) (Fig. 8) than in the scenario (S1, color in Fig. 8). These findings greatly support the importance of water availability (hydrological condition) and solar radiation intensity (meteorological condition) to boosting the synergetic benefits of the WFE nexus.

Table 4 summarized the improvement rate corresponding to the synergies of the WFE nexus created by the MOGOA solutions under the three scenarios, where the non-optimization technique served as the benchmark. The results of the solution completely dominated by PHO (Solution A) disclosed that the improvement rates of water storage (RWS) were 10.9% in the Wet plus High scenario (S3) and 7.9% in the Dry plus Low scenario (S1), the improvement rates of food production (AFP) were 6.3% in S3 and 3.3% in S1, and the improvement rates of food production (APB) reached 23.7% in S3 and 12.3% in S1. Accordingly the energy benefits (APB) achieved USD 93.9×10^6 in S3 and USD 82.23×10^6 in S1 (Fig. 8). These outcomes indicated that Solution A would substantially raise much more energy output (hydropower and floating PV) in the Wet plus High scenario (S3) than in the Dry plus Low scenario (S1). Similarly, Solution B (RWS fully dominates) and Solution C (RSD fully dominates) would significantly drive up more water storage (improvement rate = 19.6%) and more food production (improvement rate = 11.4%) in the Wet plus High scenario (S3), as compared with those

35

Table 4 Improvement rates concerning the synergistic benefits of the WFE nexus attained from the MOGOA solutions under three scenarios. The non-optimization technique served as the benchmark.

Solution (obtained from MOGOA)	Nexus	Indicator	Scenario		
			S1 Dry plus Low[e]	S2 Normal plus Moderate[f]	S3 Wet plus High[g]
Solution A (PHO[d] fully dominates)	Water	RWS[a]	7.9[h]	9.8	10.9
	Food	AFP[b]	3.3	4.9	6.3
	Energy	APB[c]	12.3	18.6	23.7
Solution B (RWS fully dominates)	Water	RWS	16.1	18.2	19.6
	Food	AFP	2.2	3.5	4.9
	Energy	APB	3.7	8.1	13.3
Solution C (RSD fully dominates)	Water	RWS	2.9	3.3	5.9
	Food	AFP	6.0	8.8	11.4
	Energy	APB	8.1	12.1	16.6
Solution D (compromised)	Water	RWS	10.2	13.6	15.2
	Food	AFP	5.5	6.9	8.1
	Energy	APB	10.1	16.0	20.5

[a] average annual ratio of water storage to reservoir capacity in the Shihmen Reservoir.

[b] average annual food production (including rice, vegetables, and fruits).

[c] average annual power benefits of the floating PV (Taoyuan City) and hydropower (Shihmen Hydropower Station).

[d] average annual floating PV and hydropower output.

[e] S1_Dry (Low) year: occurrence frequency of a dry year (low solar radiation intensity) was 80% (80%) during 2004 and 2019.

[f] S2_Normal (Moderate) year: occurrence frequency a normal year (moderate solar radiation intensity) was 50% (50%) during 2004 and 2019.

[g] S3_Wet (High) year: occurrence frequency of a wet year (high solar radiation intensity) was 20% (20%) during 2004 and 2019.

[h] Improvement rate (%), and the benchmark was the non-optimization technique.

of the Dry plus Low scenario (S1). This again demonstrated the significance of water availability and solar radiation intensity in stimulating the synergetic benefits of the WFE nexus. Furthermore, the results of Solution D pointed out that the complementary generation of hydropower (reservoir) and floating PV deployment (pond) in the Normal plus Moderate scenario (S2) could promote the water storage by as much as 13.6% (water

sector), raise food production by up to 6.9% (food sector), and run up the benefit of hydropower and floating PV by USD 86.81 million (Fig. 8), with an improvement rate of 16% (power sector). Although Solution D was a compromised solution, its high achievement in energy sectors could be accredited to the complementary collaboration between hydropower operation and floating PV deployment.

Table 5 presented the improvement rates concerning the synergies of the WFE nexus created by the MOGOA solutions, considering the impacts of the respective weights of the three objects (PHO, RWS, and RSD) based on the long-term complementary operation strategy under three scenarios. The non-optimization technique served as the benchmark. The weights of three objects not only disclosed the preference of decision-makers but also indicated the improvement rates corresponding to the synergies of the WFE nexus, where a larger weight would create a larger improvement rate. For instance, the largest improvement rate was created by the energy production with the largest weight in Solution 1 under all cases, meanwhile, similar phenomena appeared in Solutions 2-4. The results suggested with various favorable nexus solutions that decision-makers could experience potential outcomes (benefits) to make ambitious (or conservative) nexus strategies in response to challenges encountered in water, food and energy sectors under different scenarios.

In sum, the proposed MOGAO methodology aimed at exploring the collaboration between floating PV deployment on irrigation ponds and hydropower (reservoir) operation to spur on WFE nexus synergies, in comparison to the non-optimization technique. Water shortages threatening public and irrigation sectors appeared to be ameliorated by means of optimizing reservoir operation through a tradeoff between

Table 5 Improvement rates concerning the synergies of the WFE nexus created by the MOGOA solutions, which considered the impacts of the respective weights of three objects on the WFE nexus based on the long-term complementary operation strategy under three scenarios. The non-optimization technique served as the benchmark.

Solution (obtained from MOGOA)	Nexus (Weight[a])	Indicator	Scenario		
			S1	S2	S3
			Dry plus Low	Normal plus Moderate	Wet plus High
Solution 1: Benefit to PHO	Water (0.20)	RWS	4.9[b]	6.4	8.4
	Food (0.20)	AFP	4.5	5.9	7.8
	Energy (0.60)	APB	10.1	14.3	18.5
Solution 2: Benefit to RWS	Water (0.60)	RWS	11.7	14.8	17.2
	Food (0.20)	AFP	4.7	6.1	7.7
	Energy (0.20)	APB	5.4	6.5	8.1
Solution 3: Benefit to RSD	Water (0.20)	RWS	3.5	5.7	7.4
	Food (0.60)	AFP	5.7	8.3	10.9
	Energy (0.20)	APB	4.9	6.9	9.5
Solution 4: Compromised	Water (0.33)	RWS	5.4	9.1	12.1
	Food (0.33)	AFP	5.1	6.5	8.6
	Energy (0.34)	APB	7.2	9.5	14.2

[a] Weights were calculated using the standardization values of three objects (PHO, RWS, and RSD) created by the MOGOA solutions. The sum of the respective weights of three objects was equal to one.

[b] Improvement rate (%), and the benchmark was the non-optimization technique.

reservoir storage and water supply while insufficient energy production endangering urbanization development could be improved through the joint optimization of floating PV deployment and hydropower generation. The diverse MOGOA solutions could simultaneously optimize the synergetic benefits of traditional reservoir impoundment, water supply, as well as hydropower output regulated by SOP (M-5 rule curves) and solar power output from floating PV deployment. The RWS was improved by 4.3% up to 13%, the RSD by 3.6% up to 13%, and the PHO by 4.8% up to 15.1% under the multiple-year scenario (Table 1). With the optimal solutions on hand, decision-makers could reasonably select appropriate strategies to deal with various meteorological and hydrological

conditions faced for effectively managing the intensive conflicts among energy, food and water demanding sectors. Additionally, for a total irrigation pond area of roughly 12 km^2 (740 ponds) in Taoyuan City of Taiwan, the potential installed capacity (MW) would reach as high as 992 MW if each of the 740 ponds could be deployed a floating PV system over 40% of the pond area based on an assumption of homogeneous solar radiation intensity in Taoyuan City.

5. Conclusions

This study conducted a holistic assessment on the prospect for long-term complementary operation between floating photovoltaic and hydropower generation in the interest of cleaner energy development for improving water-food-energy nexus synergies by exploring a MOGOA-based approach. The hydropower reservoir operation based on M-5 rule curves and floating photovoltaic deployment using horizontal installation (tilt angle = 0°) served as the benchmark (non-optimization approach). The main conclusions were drawn as follows.

The optimal solutions under the multiple-year scenario demonstrated the average annual ratio of water storage to reservoir capacity achieved as much as 52%, the average annual food production came up with 74 million kg (corresponding to the ratio of water supply to water demand = 94%), and the average hydropower and floating photovoltaic output reached as high as 694 million kWh. The maximal improvement rates of the MOGOA-based approach could reach 13%, 13.3% and 15.1% in water storage, food production and energy output, respectively, as compared to the benchmark. The optimal tilt angles of floating photovoltaic installation would vary between -11.9° (Summer) and 44.3°

(Winter). The deployment of floating photovoltaic systems over 740 ponds would lead to a total installed capacity of 992 MW and a total installed cost of USD 942.4 million while the average annual output benefit would vary between USD 66.3 million and USD 74.8 million under the multiple-year scenario. The period of cost recovery for floating photovoltaic deployment would be 8-10 years once energy production starts. Furthermore, the complementary collaboration between floating photovoltaic and hydropower generation would make the average annual energy benefit reach high up to USD 91 million.

This study not only initiates effective actions on hydro-floating photovoltaic power operation to promote water-food-energy nexus synergies but also innovating practical solutions to renewable energy exploitation in the best interest of friendly environment and social sustainability. Future research can consider assessing more mutual benefits (e.g. carbon dioxide emission reduction and land conservation) driven by floating photovoltaic deployment at a global or national scale, apart from water-food-energy synergies.

References

[1] Zeng, X. T., Zhang, J. L., Yu, L., Zhu, J. X., Li, Z., & Tang, L. (2019). A sustainable water-food-energy plan to confront climatic and socioeconomic changes using simulation-optimization approach. Applied Energy, 236, 743–759. https://doi:10.1016/j.apenergy.2018.11.086.

[2] Wang, X.-C., Klemeš, J. J., Wang, Y., Dong, X., Wei, H., Xu, Z., et al. (2020). Water-Energy-Carbon Emissions nexus analysis of China: An environmental input-output model-based approach. Applied Energy, 261, 114431. https://doi:10.1016/j.apenergy.2019.114431.

[3] Feng, C., Qu, S., Jin, Y., Tang, X., Liang, S., Chiu, A. C. F., et al. (2019). Uncovering urban food-energy-water nexus based on physical input-output analysis: The case of the Detroit Metropolitan Area. Applied Energy, 252, 113422. https://doi:10.1016/j.apenergy.2019.113422.

[4] Fan, X., Zhang, W., Chen, W., & Chen, B. (2020). Land–water–energy nexus in agricultural management for greenhouse gas mitigation. Applied Energy, 265, 114796. https://doi:10.1016/j.apenergy.2020.114796.

[5] Chen, S., Tan, Y., & Liu, Z. (2019). Direct and embodied energy-water-carbon nexus at an inter-regional scale. Applied Energy, 251, 113401. https://doi:10.1016/j.apenergy.2019.113401.

[6] Amjath-Babu, T. S., Sharma, B., Brouwer, R., Rasul, G., Wahid, S. M., Neupane, N., et al. (2019). Integrated modelling of the impacts of hydropower projects on the water-food-energy nexus in a transboundary Himalayan river basin. Applied Energy, 239, 494–503. https://doi:10.1016/j.apenergy.2019.01.147.

[7] Fang, W., Huang, Q., Huang, S., Yang, J., Meng, E., & Li, Y. (2017). Optimal sizing of utility-scale photovoltaic power generation complementarily operating with hydropower: A case study of the world's largest hydro-photovoltaic plant. Energy Conversion and Management, 136, 161–172. https://doi:10.1016/j.enconman.2017.01.012.

[8] Mahmoudimehr, J., & Shabani, M. (2018). Optimal design of hybrid photovoltaic-hydroelectric standalone energy system for north and south of Iran. Renewable Energy, 115, 238–251. https://doi:10.1016/j.renene.2017.08.054.

[9] Liu, L., Sun, Q., Li, H., Yin, H., Ren, X., & Wennersten, R. (2019). Evaluating the benefits of integrating floating photovoltaic and pumped storage power system. Energy Conversion and Management, 194, 173–185. https://doi:10.1016/j.enconman.2019.04.071.

[10] Xu, X., Hu, W., Cao, D., Huang, Q., Chen, C., & Chen, Z. (2019). Optimized sizing of a standalone PV-wind-hydropower station with pumped-storage installation hybrid energy system. Renewable Energy. https://doi:10.1016/j.renene.2019.09.099.

[11] Wang, X., Chang, J., Meng, X., & Wang, Y. (2019). Hydro-thermal-wind-photovoltaic coordinated operation considering the comprehensive utilization of reservoirs. Energy Conversion and Management, 198, 111824. https://doi:10.1016/j.enconman.2019.111824.

[12] Wang, X., Chang, J., Meng, X., & Wang, Y. (2018). Short-term hydro-thermal-wind-photovoltaic complementary operation of interconnected power systems. Applied Energy, 229, 945–962. https://doi:10.1016/j.apenergy.2018.08.034.

[13] Farfan, J., & Breyer, C. (2018). Combining floating solar photovoltaic power plants and hydropower reservoirs: A virtual battery of great global potential. Energy Procedia, 155, 403–411. https://doi:10.1016/j.egypro.2018.11.038.

[14] Silvério, N. M., Barros, R. M., Tiago Filho, G. L., Redón-Santafé, M., Santos, I. F. S. dos, & Valério, V. E. de M. (2018). Use of floating PV plants for coordinated operation with hydropower plants: Case study of the hydroelectric plants of the São Francisco River basin.

Energy Conversion and Management, 171, 339–349. https://doi:10.1016/j.enconman.2018.05.095.

[15] Spencer, R. S., Macknick, J., Aznar, A., Warren, A., & Reese, M. O. (2018). Floating PV: Assessing the technical potential of photovoltaic systems on man-made water bodies in the continental U.S. Environmental Science & Technology, 1-29. https://doi:10.1021/acs.est.8b04735.

[16] Liu, L., Wang, Q., Lin, H., Li, H., Sun, Q., & wennersten, R. (2017). Power generation efficiency and prospects of floating photovoltaic systems. Energy Procedia, 105, 1136–1142. https://doi:10.1016/j.egypro.2017.03.483.

[17] Sahu, A., Yadav, N., & Sudhakar, K. (2016). Floating photovoltaic power plant: A review. Renewable and Sustainable Energy Reviews, 66, 815–824. https://doi:10.1016/j.rser.2016.08.051.

[18] Ranjbaran, P., Yousefi, H., Gharehpetian, G. B., & Astaraei, F. R. (2019). A review on floating photovoltaic (FPV) power generation units. Renewable and Sustainable Energy Reviews, 110, 332–347. https://doi:10.1016/j.rser.2019.05.015.

[19] Cazzaniga, R., Cicu, M., Rosa-Clot, M., Rosa-Clot, P., Tina, G. M., & Ventura, C. (2018). Floating photovoltaic plants: Performance analysis and design solutions. Renewable and Sustainable Energy Reviews, 81, 1730–1741. https://doi:10.1016/j.rser.2017.05.269.

[20] Rosa-Clot, M., Tina, G. M., & Nizetic, S. (2017). Floating photovoltaic plants and wastewater basins: an Australian project. Energy Procedia, 134, 664–674. https://doi:10.1016/j.egypro.2017.09.585.

[21] Rauf, H., Gull, M. S., & Arshad, N. (2019). Integrating floating solar PV with hydroelectric power plant: Analysis of Ghazi Barotha reservoir in Pakistan. Energy Procedia, 158, 816–821. https://doi:10.1016/j.egypro.2019.01.214.

[22] IRENA (2019), Renewable Energy Statistics 2019, The international renewable energy agency, Abu Dhabi. https://www.polity.org.za/article/renewable-energy-statistics-2019-2019-07-08.

[23] Mina Mesbahi, Solarplaza. Top 100 floating solar projects. https://www.solarplaza.com/channels/markets/11968/top-100-floating-solar-projects/ (accessed 24th Jan. 2019).

[24] Zhang, Y., Ma, C., Lian, J., Pang, X., Qiao, Y., & Chaima, E. (2019). Optimal photovoltaic capacity of large-scale hydro-photovoltaic complementary systems considering electricity delivery demand and reservoir characteristics. Energy Conversion and Management, 195, 597–608. https://doi:10.1016/j.enconman.2019.05.036.

[25] Ming, B., Liu, P., Guo, S., Cheng, L., & Zhang, J. (2019). Hydropower reservoir reoperation to adapt to large-scale photovoltaic power generation. Energy, 179, 268–279. https://doi:10.1016/j.energy.2019.04.209.

[26] Ming, B., Liu, P., Guo, S., Cheng, L., Zhou, Y., Gao, S., et al. (2018). Robust hydroelectric unit commitment considering integration of large-scale photovoltaic power: A case study in China. Applied Energy, 228, 1341–1352. https://doi:10.1016/j.apenergy.2018.07.019.

[27] Li, H., Liu, P., Guo, S., Ming, B., Cheng, L., & Yang, Z. (2019). Long-term complementary operation of a large-scale hydro-photovoltaic hybrid power plant using explicit stochastic optimization. Applied Energy, 238, 863–875. https://doi:10.1016/j.apenergy.2019.01.111.

[28] Jurasz, J., & Ciapała, B. (2017). Integrating photovoltaics into energy systems by using a run-off-river power plant with pondage to smooth energy exchange with the power gird. Applied Energy, 198, 21–35. https://doi:10.1016/j.apenergy.2017.04.042.

[29] Haas, J., Khalighi, J., de la Fuente, A., Gerbersdorf, S. U., Nowak, W., & Chen, P.-J. (2020). Floating photovoltaic plants: Ecological impacts versus hydropower operation flexibility. Energy Conversion and Management, 206, 112414. https://doi:10.1016/j.enconman.2019.112414.

[30] Uri Stiubiener, Thadeu Carneiro da Silva, Federico Bernardino Morante Trigoso, Ricardo da Silva Benedito, Julio Carlos Teixeira. (2020). PV power generation on hydro dam's reservoirs in Brazil: A way to improve operational flexibility. Renewable Energy, 150, 765-776. https://doi.org/10.1016/j.renene.2020.01.003.

[31] Château, P.-A., Wunderlich, R. F., Wang, T.-W., Lai, H.-T., Chen, C.-C., & Chang, F.-J. (2019). Mathematical modeling suggests high potential for the deployment of floating photovoltaic on fish ponds. Science of The Total Environment. 687, 654-666. https://doi:10.1016/j.scitotenv.2019.05.420.

[32] Yang, Y., Zhou, J., Liu, G., Mo, L., Wang, Y., Jia, B., et al. (2020). Multi-plan formulation of hydropower generation considering uncertainty of wind power. Applied Energy, 260, 114239. https://doi:10.1016/j.apenergy.2019.114239.

[33] Wang, X., Virguez, E., Kern, J., Chen, L., Mei, Y., Patiño-Echeverri, D., et al. (2019). Integrating wind, photovoltaic, and large hydropower during the reservoir refilling period. Energy Conversion and Management, 198, 111778. https://doi:10.1016/j.enconman.2019.111778.

[34] Wang, F., Xie, Y., & Xu, J. (2019). Reliable-economical equilibrium based short-term scheduling towards hybrid hydro-photovoltaic generation systems: Case study from China. Applied Energy, 253, 113559. https://doi:10.1016/j.apenergy.2019.113559.

[35] Dujardin, J., Kahl, A., Kruyt, B., Bartlett, S., & Lehning, M. (2017). Interplay between photovoltaic, wind energy and storage hydropower in a fully renewable Switzerland. Energy, 135, 513–525. https://doi:10.1016/j.energy.2017.06.092.

[36] Liu, W., Zhu, F., Chen, J., Wang, H., Xu, B., Song, P., et al. (2019). Multi-objective optimization scheduling of wind–photovoltaic–hydropower systems considering riverine ecosystem. Energy Conversion and Management, 196, 32–43. https://doi:10.1016/j.enconman.2019.05.10.

[37] Uen, T.-S., Chang, F.-J., Zhou, Y., & Tsai, W.-P. (2018). Exploring synergistic benefits of Water-Food-Energy Nexus through multi-objective reservoir optimization schemes. Science of The Total Environment, 633, 341–351. https://doi:10.1016/j.scitotenv.2018.03.172.

[38] Zhou, Y., Chang, L.-C., Uen, T.-S., Guo, S., Xu, C.-Y., & Chang, F.-J. (2019). Prospect for small-hydropower installation settled upon optimal water allocation: An action to stimulate synergies of water-food-energy nexus. Applied Energy, 238, 668–682. https://doi:10.1016/j.apenergy.2019.01.069.

[39] Zhou, Y., Guo, S., Hong, X., & Chang, F.-J. (2017). Systematic impact assessment on inter-basin water transfer projects of the Hanjiang River Basin in China. Journal of Hydrology, 553, 584–595. https://doi:10.1016/j.jhydrol.2017.08.039.

[40] Mirjalili, S. Z., Mirjalili, S., Saremi, S., Faris, H., & Aljarah, I. (2017). Grasshopper optimization algorithm for multi-objective optimization problems. Applied Intelligence, 48(4), 805–820. https://doi:10.1007/s10489-017-1019-8.

[41] Saremi, S., Mirjalili, S., & Lewis, A. (2017). Grasshopper Optimisation Algorithm: Theory and application. Advances in Engineering Software, 105, 30–47. https://doi:10.1016/j.advengsoft.2017.01.004

[42] Deb, K., Pratap, A., Agarwal, S., & Meyarivan, T. (2002). A fast and elitist multiobjective genetic algorithm: NSGA-II. IEEE Transactions on Evolutionary Computation, 6(2), 182–197. https://doi:10.1109/4235.996017.

[43] Coello CC, Lechuga MS (2002). MOPSO: A proposal for multiple objective particle swarm optimization. In: Proceedings of the 2002 congress on evolutionary computation, 2002. CEC'02, 1051-1056.

[44] Alaya I, Solnon C, Ghedira K (2007). Ant colony optimization for multi-objective optimization problems. In: ICTAI (1), 450-457.

[45] Xue F, Sanderson AC, Graves RJ (2003). Pareto-based multiobjective differential evolution. In: The 2003 congress on evolutionary computation, 2003. CEC'03, 862–869.

[46] Knowles JD, Corne DW(2000). Approximating the nondominated front using the Pareto archived evolution strategy. Evolutionary Computation, 8:149-172. http://doi:10.1162/106365600568167.

[47] World Bank Group; Energy Sector Management Assistance Program; Solar Energy Research Institute of Singapore. 2019. Where sun meets water: floating solar market report. World Bank, Washington, DC. © World Bank. https://openknowledge.worldbank.org/handle/10986/31880.

Credit Author Statement

Yanlai Zhou: Data curation, Formal analysis, Software, Validation, Writing-original draft. **Fi-John Chang:** Funding acquisition, Methodology, Project administration, Supervision, Writing-review & editing. **Li-Chiu Chang:** Methodology, Project administration, Resources, Supervision. **Wei-De Lee:** Data analysis, Formal analysis. **Angela Huang:** Data analysis, Visualization. **Chong-Yu Xu:** Methodology, Writing-review & editing. **Shenglian Guo:** Methodology, Writing-review & editing.

Declaration of interests

� The authors declare that they have no known competing financial interests or personal relationships that could have appeared to influence the work reported in this paper.

☐The authors declare the following financial interests/personal relationships which may be considered as potential competing interests: